Effect of alloy temper on surface modification of aluminium 2624 by laser shock peening

Zabeen, S., Langer, K. & Fitzpatrick, M. E.

Original citation & hyperlink:
Zabeen, S, Langer, K & Fitzpatrick, ME 2018, 'Effect of alloy temper on surface modification of aluminium 2624 by laser shock peening' Surface and Coatings Technology, vol. 347, pp. 123-135.
https://dx.doi.org/10.1016/j.surfcoat.2018.04.069

DOI 10.1016/j.surfcoat.2018.04.069
ISSN 0257-8972
ESSN 1879-3347

Publisher: Elsevier

Effect of alloy temper on surface modification of aluminium 2624 by laser shock peening

S. Zabeen[1], K. Langer[2], and M. E. Fitzpatrick[1]

[1] *Coventry University, Faculty of Engineering, Environment and Computing, Gulson Road, Coventry, CV1 2JH, UK*

[2]*Air Force Research Laboratory, Wright-Patterson Air Force Base, OH 45433, USA*

Email: Michael.Fitzpatrick@coventry.ac.uk

Abstract

We have investigated the hardening response, residual stress generation and microstructural changes in aluminium alloy 2624 owing to laser shock peening. The alloy was studied in two heat treatment conditions, T351 and T39, that have 20% difference in yield strength: hence the effects of laser power density and multiple peen impacts on materials with nominally identical physical properties but with different hardening responses has been studied. Hardness was characterised by nanoindentation, and residual stresses were measured by incremental hole drilling.

The magnitude and the depth of the peak compressive residual stresses increase with increasing power densities as well as the number of laser impacts, before reaching a saturation point above which loss of surface compression occurs. Maximum compressive residual stresses were around –350 MPa, and maximum hardness increase was around 22%. The treatment has a noticeable effect in changing the microstructures of the T351 temper while the T39 remained almost unchanged.

1. Introduction

Laser shock peening (LSP) is a surface processing technology that offers life extension of metallic structural components for aerospace, automotive, and power generation industries, among others, by inducing deep compressive residual stresses that improve strength, hardness, fatigue life and corrosion resistance of the material [1, 2]. Fatigue life improvement via LSP is largely dependent on the residual stress generated, which in turn is dependent upon the peening parameters. A number of researchers have reported the effect of LSP on the mechanical properties, residual stress, and the resulting life improvement of various aluminium alloys. The peak compressive residual stresses for Al 2024 T3 were reported as around –150 MPa at a power density of 3 GW/cm^2 [3], and about –180 and –300 MPa at 1 and 4 GW/cm^2, respectively [4]. Sano *et al*. [5] also reported peak residual stress of –300 MPa and hardness of about 2.4 GPa for the same alloy, although a different laser system was used.

Al 2624 is a newly developed alloy (to replace Al 2024) that has improved fracture toughness and damage tolerance compared to Al 2024. At present, developing an LSP-based fatigue design for enhanced structural integrity relies heavily on trial-and-error without a detailed understanding of the correlation between the plastic deformation and the consequent hardening and generation of residual stress. It is therefore costly and time-consuming. Although efforts have been made previously to understand the effect of laser treated area on the residual stress and fatigue [6], a systematic study on the effect of single vs. multiple peen overlaps at different peening intensities, and their effects on the elastoplastic response is still lacking.

The goals of the current research are to quantify the relationships between peening conditions, induced residual stresses, hardness, and material state for aluminium 2624. We investigate the effect of peening intensity and the number of impacts on the hardness and residual stress in Al 2624 alloy in the T351 and the T39 heat treatment conditions. Two heat treatment conditions were selected to study the effects of yield strength and hardening capacity while maintaining nominally identical elastic properties.

2. Materials and Experimental Methods

2.1 Materials

Al 2624 alloy was supplied by Alcoa in two heat treatment conditions (T351 & T39). T351 alloy is solution heat-treated, stress-relieved by stretching, and naturally-aged; T39 is cold-worked and naturally-aged after solution heat treatment. The materials were received as plates with a thickness of 25 mm. The test coupons for residual stress measurement were $70 \times 70 \times 12.5$ mm^3 (see Figure 1). The specimens were extracted using wire electro-discharge machining (EDM). Since a smooth surface finish was required for peening, a surface finish of R_a = 1 was achieved using EDM skim cut settings.

The microstructure of the Al2624 in the T351 and T39 conditions is given in Figures 2a and b, respectively. Both materials have elongated grains along the rolling direction.

Figure 3 shows the quasistatic stress-strain curves supplied by Alcoa for the two heat treatment conditions, giving the elastic-plastic properties shown in Table 3. The 25% higher yield strength in the T39 as compared to the T351 is a result of the pre-deformation before natural aging.

Laser shock peening was conducted by Metal Improvement Company, Earby, UK using the peening parameters shown in Table 2. Each specimen was peened in four locations (Figure 1), with each location receiving identical treatment. This allowed for four measurement locations per specimen. Peening was applied with square spots using a fixed-energy laser system (13 J) resulting in different spot sizes for different laser intensities. A pulse duration of 18 ns was used throughout.

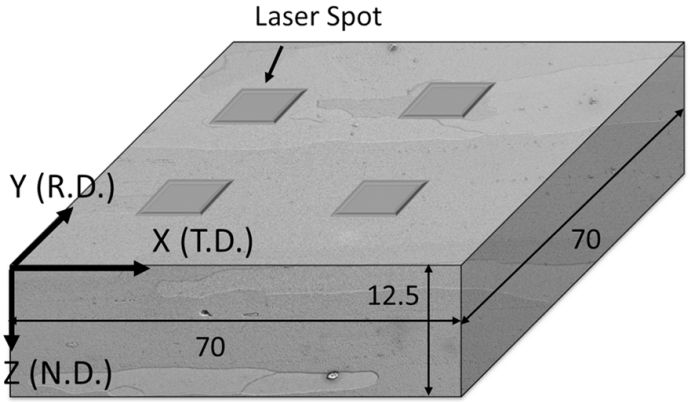

Figure 1: Schematic of the test coupon for residual stress measurement, showing four laser peen spots. All dimensions are in millimetres. R.D., T.D., and N.D. refer to the rolling, transverse and normal directions.

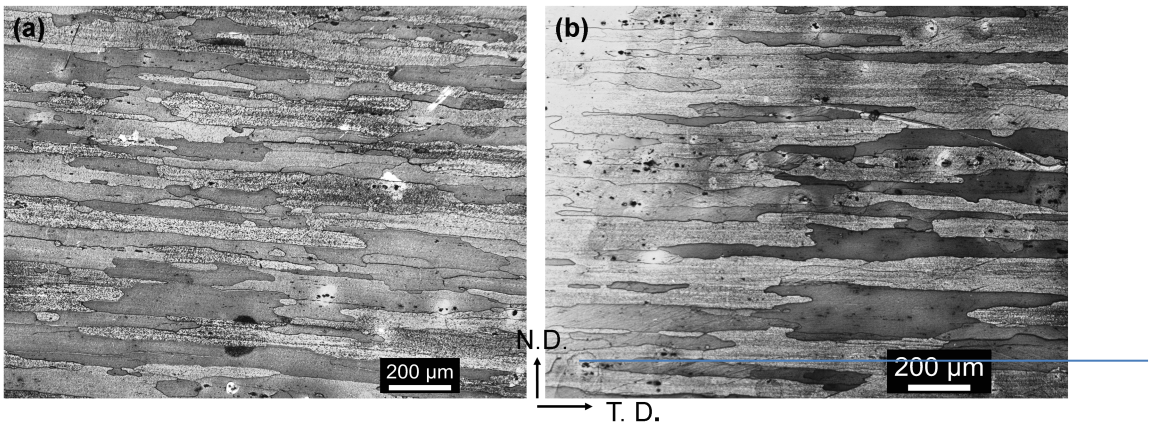

Figure 2: Microstructure of Al-2624 alloy showing elongated grains in the rolling direction, (a) for T351 and (b) T-39 heat treatment condition.

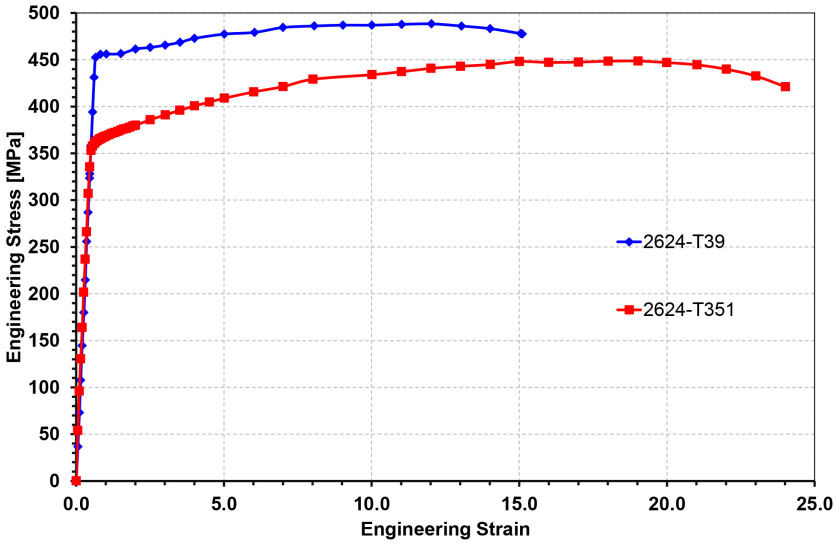

Figure 3: Stress–strain curve for Al-2624 alloy in T351 and T39 conditions. Data courtesy Dr M. Heinimann, Alcoa Inc. (now Arconic).

Table 1: Elastic-Plastic Properties of Al-2624 alloy in T351 and T39 conditions

Heat Treatment	Elastic Modulus / GPa	Yield Strength σ_y / MPa	E / σ_y	Ultimate Tensile Strength / MPa	Strain to failure / %
T351	70	360	194	448	24
T39	70	450	155	487	15

Table 2: Peening parameters used in this study

Material	Power Density-Pulse duration-# Impacts / GW/cm^2-ns-#	Spot Dimensions / mm^2
Al-2624 T351	1-18-1	8.5 × 8.5
	1-18-2	
	1-18-4	
	1-18-7	
	3-18-1	5 × 5
	3-18-2	
	3-18-4	
	3-18-7	
	6-18-1	3.5 × 3.5
	6-18-2	
	6-18-4	
	6-18-7	
Al-2624 T39	1-18-1	8.5 × 8.5
	1-18-2	
	1-18-4	
	1-18-7	
	3-18-1	5 × 5
	3-18-2	
	3-18-4	
	3-18-7	
	6-18-1	3.5 × 3.5
	6-18-2	
	6-18-4	
	6-18-7	

2.2 Incremental Hole Drilling

Hole drilling is a fast, straightforward, and inexpensive method for residual stress measurement in the laboratory. As the name implies, in this technique a hole is drilled into the specimen, causing elastic stress relaxation as material is removed. The elastic stress relaxation causes a change in displacement in the surrounding material that is measured by a strain gauge array attached to the specimen. The residual stresses are then calculated from the measured displacements.

Hole drilling measurements were carried out using equipment developed by Stresscraft, UK. For accurate measurement the UK NPL Good Practice Guide No. 53 and ASTM E837-13a standards were followed [7, 8]. Vishay strain gauges with the specification of CEA-13-062UL-120 and EA-13-062RE-120 were used. A 2-mm-diameter hole was drilled in an orbital motion with four increments of 32 μm, four increments of 64 μm, and eight increments of 128 μm, for a total of 16 increments and a total depth of 1.4 mm.

2.3 Nanoindentation

The instrumented nanoindentation technique for hardness measurement has an advantage over traditional methods such as Vickers hardness method because it provides continuous load-displacement data as the indent is made. The technique also provides mechanical properties at a sub-millimetre level which is particularly suitable for characterisation of near-surface variations in property. Residual stresses can also be extracted, as has been shown both theoretically [9] and experimentally [10, 11].

In this study, the Oliver and Pharr method [12] was employed to calculate hardness from the load-displacement curve. From a nanoindentation test (Figure 4a) a load-depth curve as shown in Figure 4b is obtained, where h_{max} is the depth at maximum load, h_f is the final depth of penetration and h_c is the elastic contact depth.

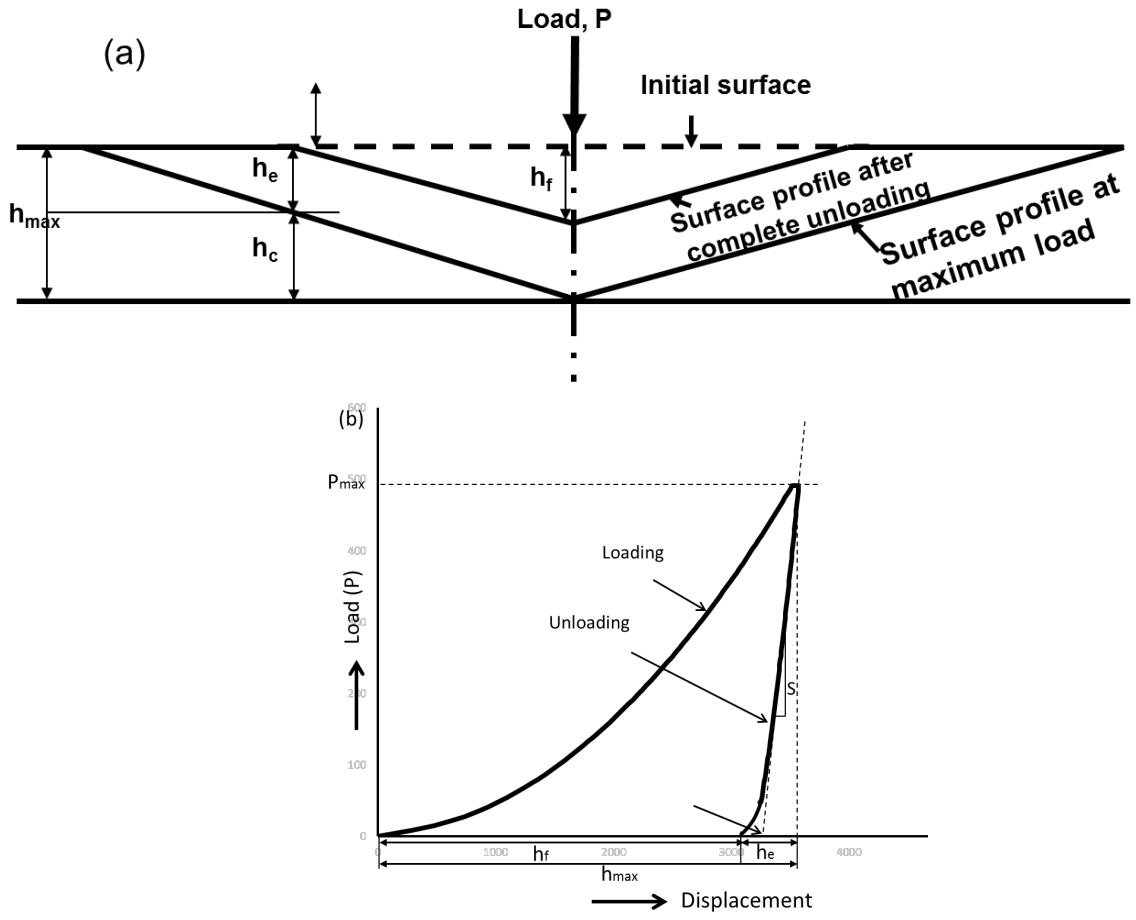

Figure 4: (a) Schematic of the indentation process and (b) load–displacement curve

A maximum indentation depth of h_{max} is achieved at maximum indentation load P_{max}. Upon unloading the material elastically recovers to a depth of h_f (Figure 4a). The

difference between the depth at maximum load and the final depth after the material is recovered is generally defined as the elastic recovery, $h_e = h_{max} - h_f$. Materials with higher yield strength will show higher elastic recovery following indentation. The ratio h_e / h_{max} is related to the elastic behaviour of the material and may be the most suitable parameter to study the response to different peening parameters.

2.3.1 Indentation procedure

All specimens were prepared by cutting using electro-discharge machining (EDM) along the centreline of the laser spot in the rolling (x) direction, then mounted in resin and ground and polished to a submicron finish using oxide particle suspension. Specimens were vibratory polished for eight hours to remove the plastically deformed material from the surface associated with polishing. Figure 5 shows a schematic representation of the EDM cut and the measurement line with respect to the cross-section of the specimen.

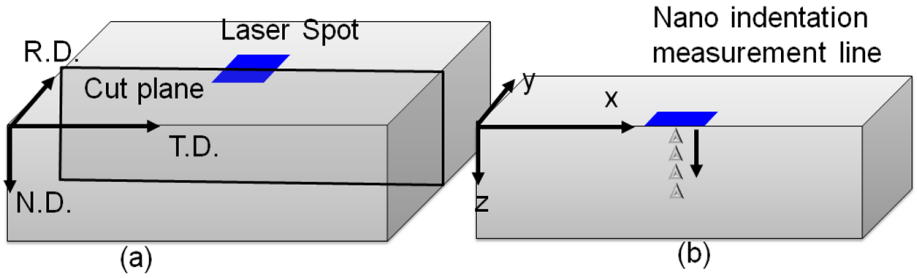

Figure 5: Schematic representations of (a) nanoindentation specimen preparation and (b) measurement line with respect to the cross-sectional area. Axes as figure 1.

For each specimen two lines of 70 indents each were made with 100 µm spacing between the indents, as shown by the larger triangular indents in Figure 6a (the smaller indents were used for validation). Figure 6b shows the surface profile of an indent made by 50 gf load, and Figures 6c and d show the corresponding line profiles along the x and z axis respectively. The depth of the indent made by the 50 gf load ranged from 2-3.5 µm depending on the peening parameters, and the height of the pileup material was between 0.2-0.5 µm (see Figure 6d).

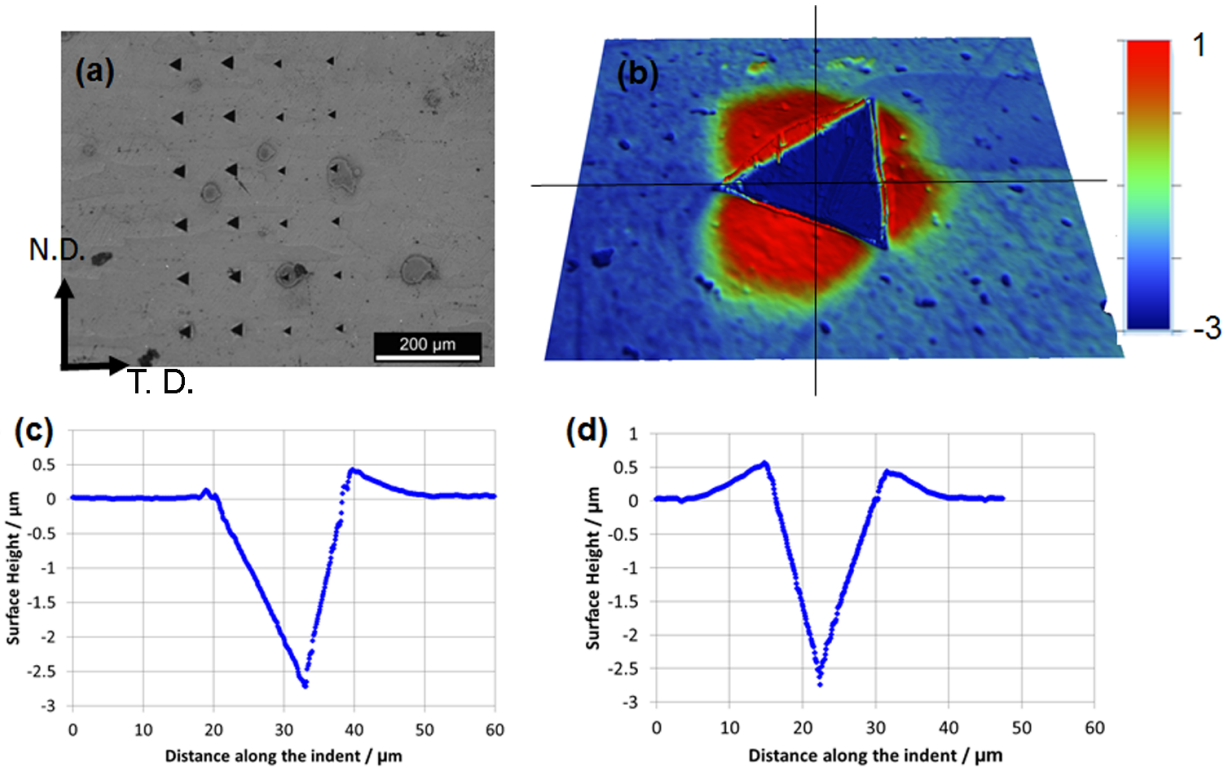

Figure 6: (a) Scanning electron micrographs showing the lines of indents; (b) surface profile of an indent created at 50 gf load; (c) line profile (along the x axis) of the indent shown in (b); and (d) line profile along the z axis

The instrument was operated in basic hardness load-displacement mode, which records load and displacement as a function of time. The indentation measurement was performed with the "Continuous Stiffness Measurement'' option that allows continuous measurement of the contact stiffness during loading. Specimens were tested with 50 gf peak load.

2.4 Microstructural characterization

Polished and indented specimens were etched with Keller's reagent for optical microscopy. Selected unetched specimens were characterized by Electron Back Scatter Diffraction using a Zeiss Sigma 500 VP field-emission gun scanning-electron microscope.

3. Results

3.1 Surface profile

The surface deformation following laser peening was measured using a Bruker ContourGT interferometer microscope. The measurement accuracy was estimated to be about 0.3 microns. Figure 7 shows the 2D surface profiles of specimens peened with condition 3-18-7 (using the standard terminology for laser peening: a-b-c, where a = Power density in GW/cm^2; b = pulse duration in ns; c= number of impacts) for T351 and T39. The laser spot size was 5 $\times$ 5 mm^2. The average depth of the peened spot is 57 μm for T351 and 44 μm for T39. The material surfaces within the peened spots are non-uniform for both materials.

Line profiles for single-spot peened specimens are plotted in Figures 8a and b for T351 and T39, respectively, to show the effect of power density (1, 3 and 6 GW/cm^2) on the depression depth, as well as the material pile-up at the edges of the laser spot. For both tempers, the average depth of the depression increases linearly with increasing intensity, and becomes slightly non-uniform (by ~5 μm) at the highest intensity used in this study (6 GW/cm^2). Compared to T351, a slightly lower deformation depth was found for the T39: for example, at the 3-18-1 peening condition, the maximum averaged depths are 10 μm and 8 μm for the T351 and the T39, respectively. This 20% lower depth in the latter is almost certainly a consequence of the higher yield strength of T39.

Figures 8c and d show the depression depth as a function of number of impacts at 6 GW/cm^2. Three features are evident in the Figure:

1) The average depression depth, *d*, as well as the height of the pileups increase with the number of impacts, *N*, for both alloys; as shown in Figure 8e, a linear relationship was observed between *d* and *N*.

2) As the number of peen layers increases, the depth profiles become increasingly more non-uniform.

3) The average depression depth in the T39 is 15% lower than the T351 at 6-18-7 (see Figure 8e). This is associated to the higher yield stress of the T39.

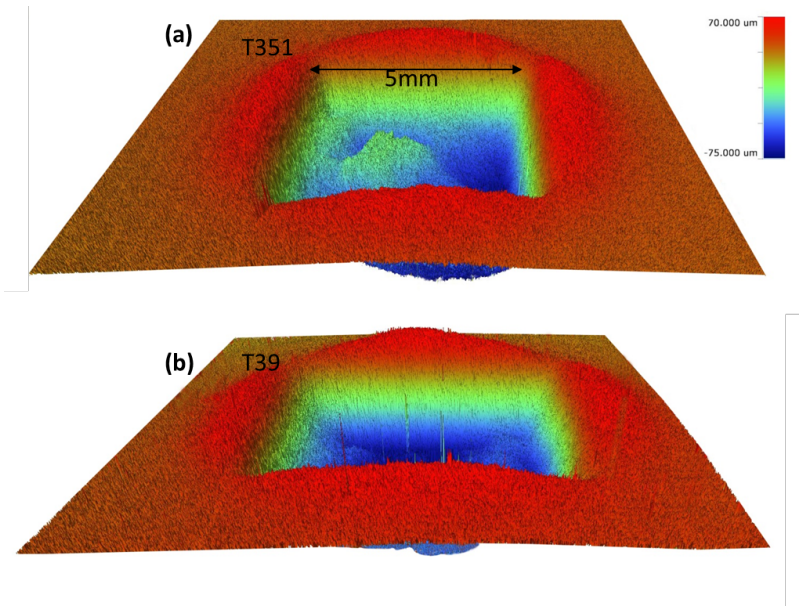

Figure 7: 2D surface profile of specimens peened with 7 hits at 3 GW cm^{-2} for 18 ns (3-18-7): (a) T351 and (b) T39. The nominal spot size is 5 × 5 mm^2

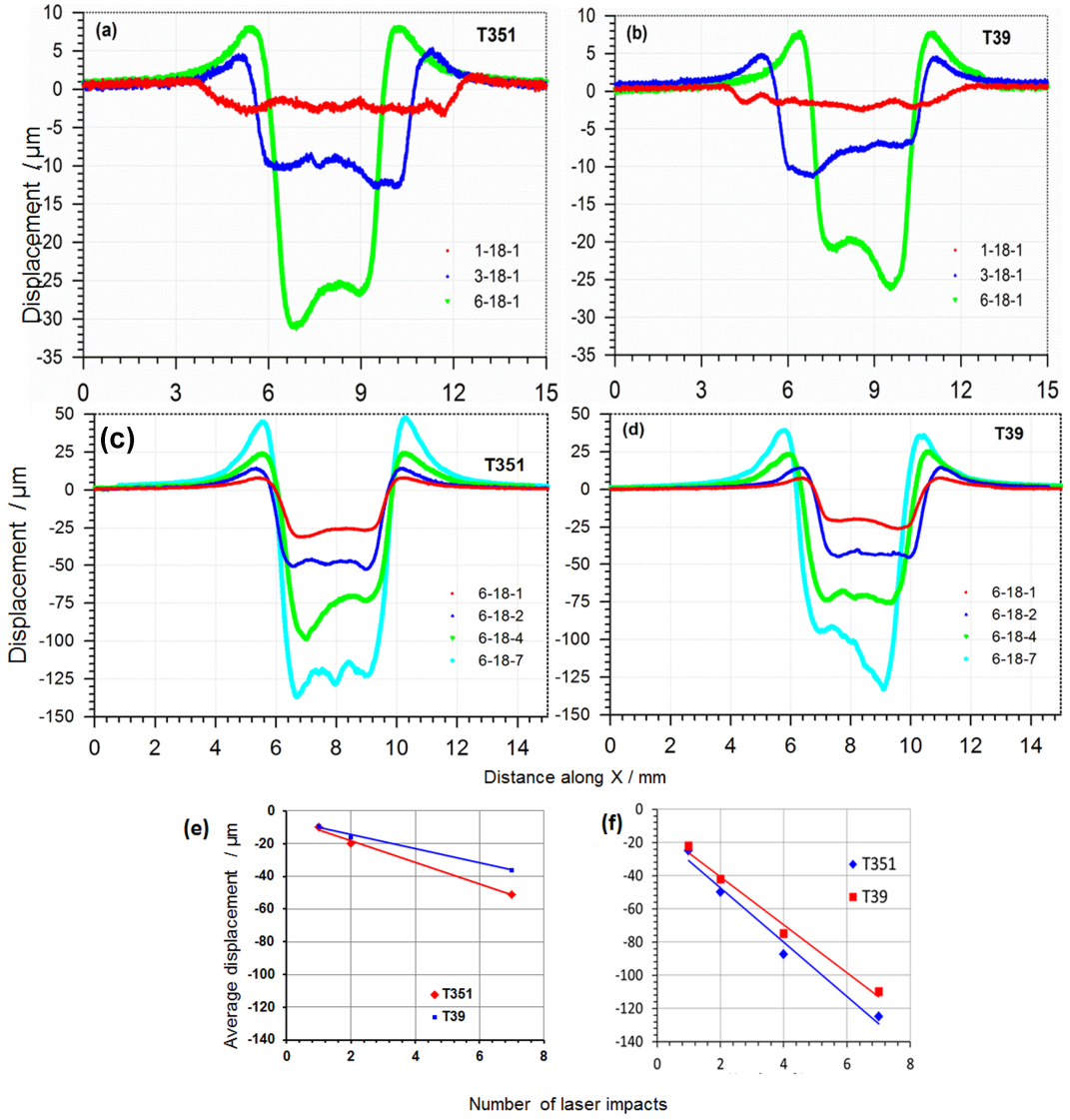

Figure 8: Effect of power density on the surface profiles of single spots peened with 1, 3, and 6 GW/cm^2: (a) T351 and (b) T39; Effect of number of impacts on the surface profile of single spots peened with 6 GW/cm^2 for (c) GW/cm^2 T351 and (d) T39 alloy; (e, f) Effect of number of layers on the depth of the spots peened with (e) 1-18-n and (f) 6-18-n

3.2 Residual stress distributions

The near-surface residual stress distributions in the T351 were measured using incremental hole drilling in as-received and electro-discharge-machined conditions prior to peening. As shown in Figure 9, the near-surface residual stress in the as-received material was about 30 MPa tensile; after EDM the surface stress was about –80 MPa compressive.

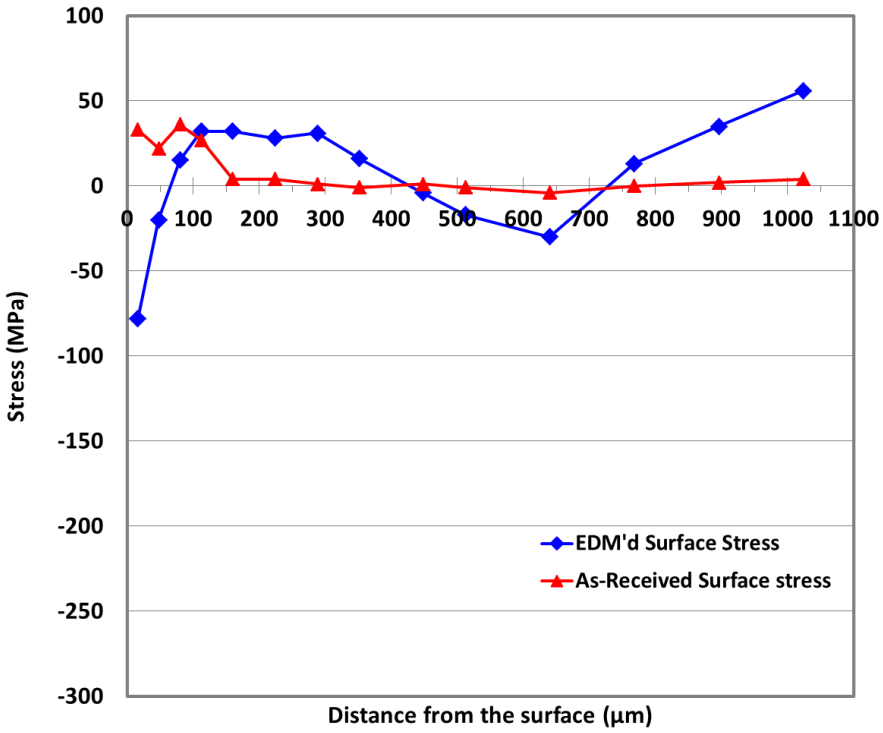

Figure 9: Surface residual stress distribution as a function of depth in the Al2624 T351 alloy in as-received and EDM surfaces before peening.

The effect of the number of laser impacts at 1 GW/cm^2 is presented in Figure 10a for T351. Following a single shot, a maximum compressive residual stresses of –220 MPa was measured at a depth of 16 µm. For two and four impacts the maximum compression shifted deeper (100-150 µm). After 7 shots, the highest compressive residual stress was measured, with a surface value of –240 MPa and a peak value of about –290 MPa at a depth of 110 µm. The higher compressive residual stresses after one impact, compared to those of two and four impacts (Figure 10a and b) may be the result of the initial residual stresses left from the EDM process.

Similar plots of the residual stresses in the T351 specimens at 3 GW/cm^2 and 6 GW/cm^2 are shown in Figures 10b and c, respectively. At both power densities, the magnitude of the compressive residual stress increases as the number of shocks increase, up to four impacts. However, at 6 GW/cm^2, near-surface residual stress relaxation (~60% compared to 3 GW/cm^2) was observed, which is likely to be a consequence of reverse yielding. This is further explained in section 4.1.

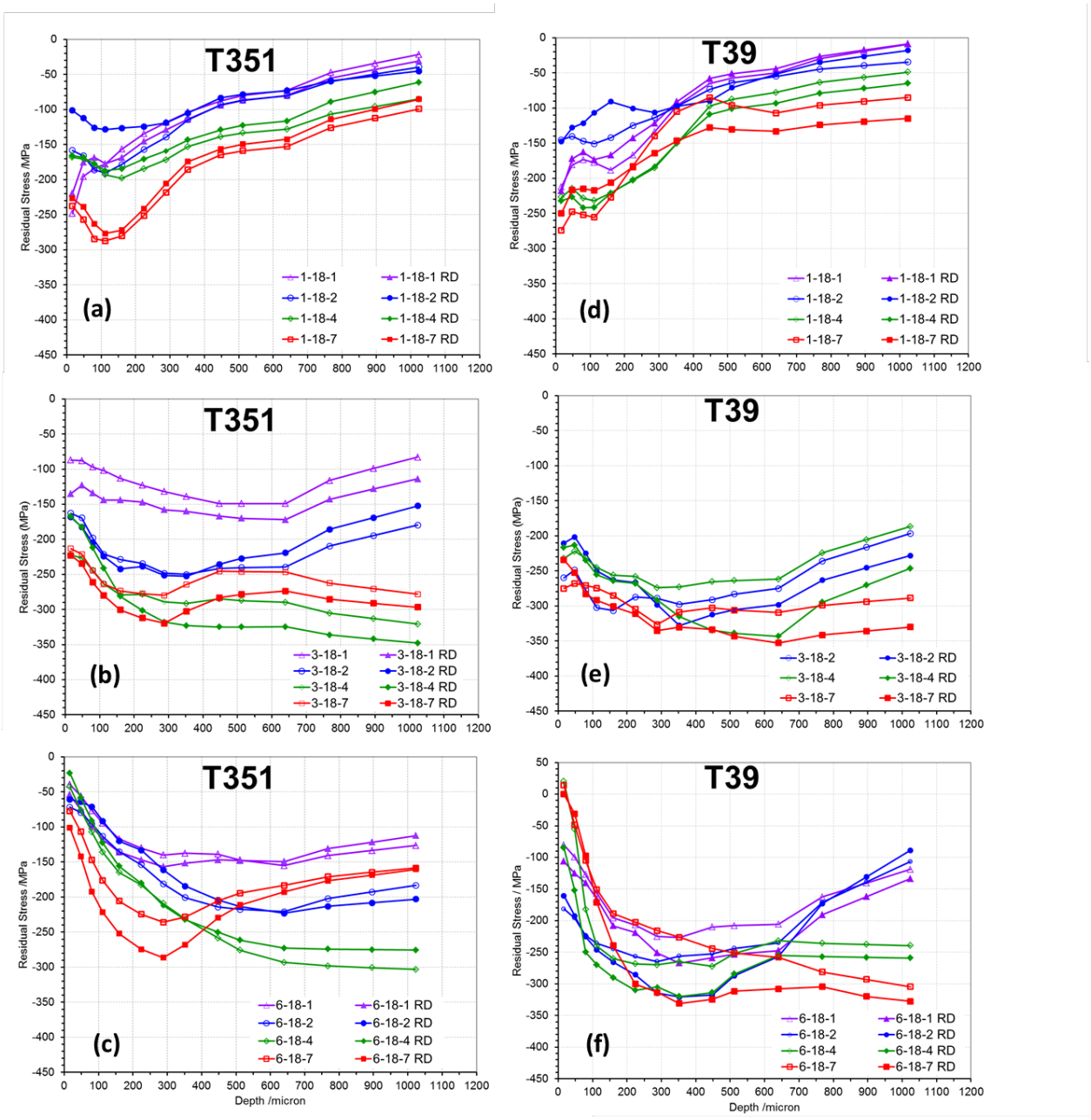

Figure 10: Residual stress profiles measured by incremental hole drilling showing the effect of number of impacts for T351 alloy at: (a) 1 GW/cm^2 (b) 3 GW/cm^2, and (c) 6 GW/cm^2; and for T39 alloy at (d) 1 GW/cm^2 (e) 3 GW/cm^2, and (f) 6 GW/cm^2 . Open and closed symbols are used for residual stresses in the transverse and rolling directions, respectively.

Residual stresses for the T39 are shown in Figures 10d-f. At the lowest power density (1-18-1) (Figure 10d), the maximum compression is at the surface, whilst for the higher power densities, the peak compression is sub-surface. For the most severe peening (6-18-7), the surface stress becomes slightly tensile.

3.3 Microstructural characterization

Figure 11 shows how the microstructure of both materials is affected by laser shock peening. Comparison between the unpeened (Figure 11a) and peened (with 1-18-7, Figure 11b) T351 shows clear evidence of grain refinement near-surface in the peened specimen. The extent of the grain refinement zone is ~3.5 mm from the peened surface and a grain size gradient exists with the smallest grain size near the surface. In contrast to the T351, no grain refinement is apparent in the T39 (Figure 11d) at the equivalent peening condition. This may be due to the prior deformation in the T39.

Smaller grains in the T351 condition were also found after a single impact at 1 GW/cm^2, as shown in Figure 12a. The grains are elongated in the transverse direction but refined to a smaller size than in the unpeened material. The average grain size along the transverse direction is 175 μm whereas that for unpeened material is ~500 μm (see Figure 2a). In comparison to the T351, grain size refinement is again not apparent in the T39 material (Figure 12c).

Increasing the power density from 1 to 3 GW/cm^2 did not result in any further grain size refinement in the T351. However, when the power density was increased to 6 GW/cm^2 the average grain size along the transverse direction was further reduced (Figure 12b). In addition, subgrain boundaries are visible within the darker grains which are likely a result of the increased plastic deformation.

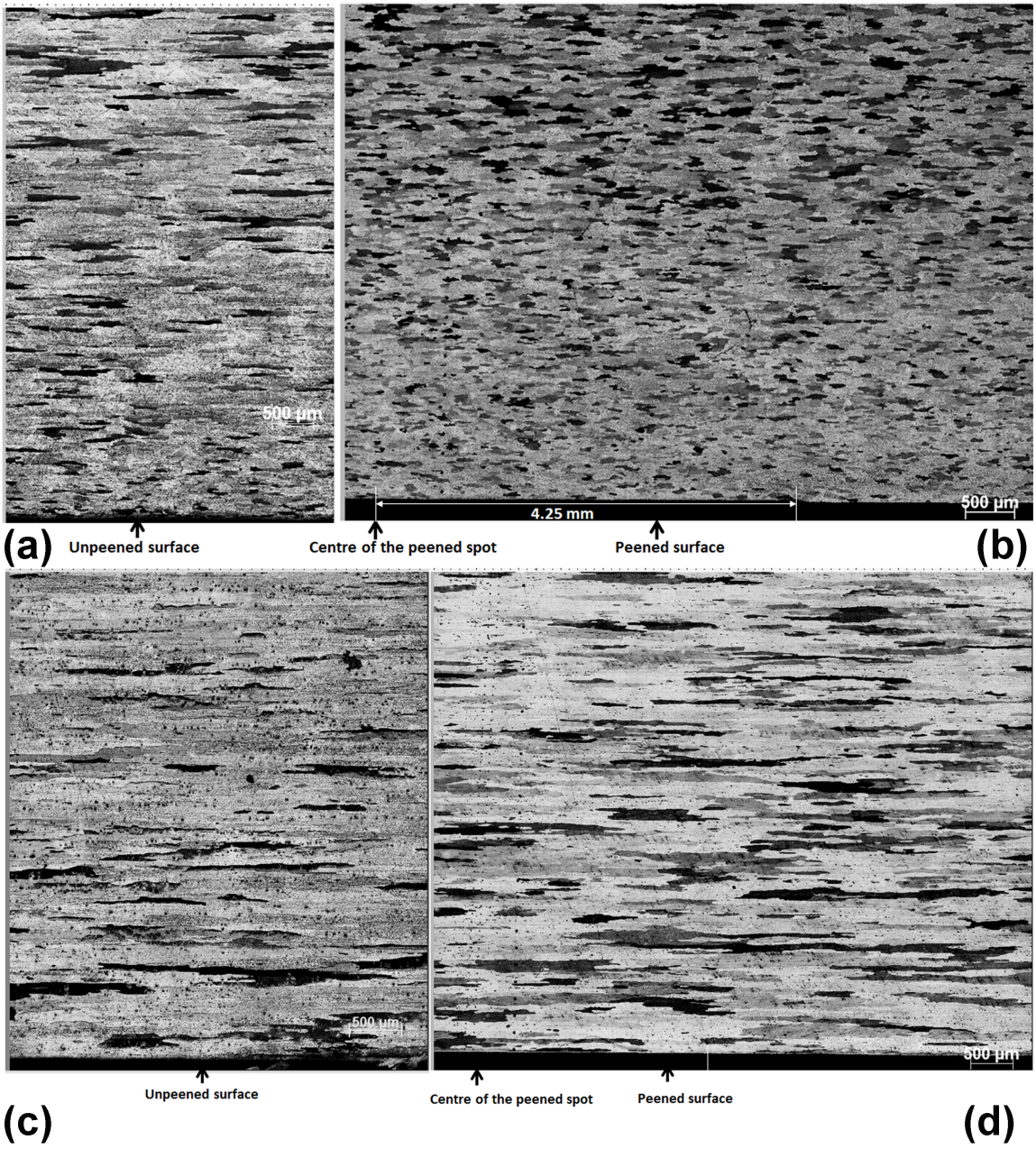

Figure 11: Microstructural images for the (a) unpeened T351; (b) peened (1-18-7) T351; (c) unpeened T39; and (d) peened (1-18-7) T39.

At the highest power density (6 GW/cm^2) studied here, evidence of a recast layer was found for the T39 material as shown in Figure 12d. This means that the temperature at the surface of the specimens reached the melting point. The thickness of the recast layer is 100 µm. Formation of the recast layer can be correlated with the reduced compressive residual stresses near the surface (Figure 10f).

Laser-peening-induced grain refinement in the T351 was confirmed by the electron back scattered diffraction (EBSD) map given in Figure 13 for 6-18-1. The average grain size measured from the EBSD map is about 100 microns in the transverse direction.

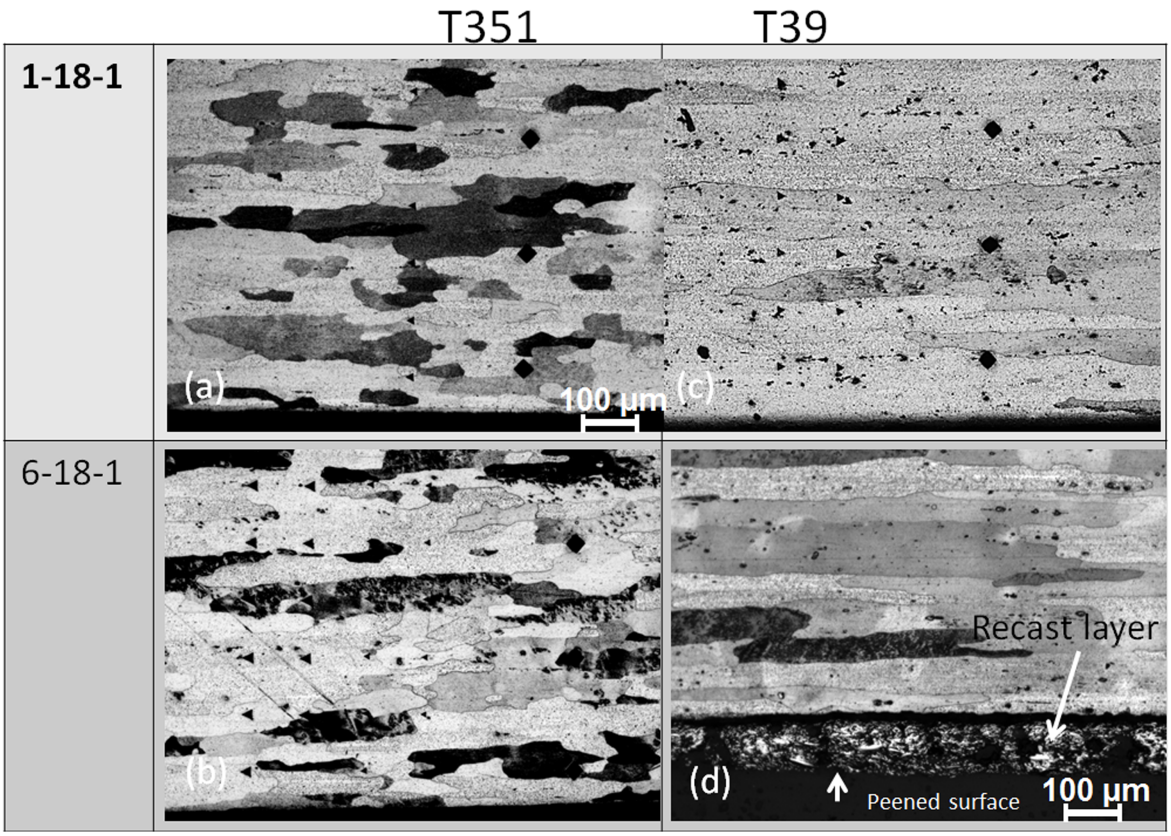

Figure 12: Optical images for the T351 (a-b), and the T39 (c-d) showing the effect of power density for a single impact. Both Vickers and instrumented indention marks can be seen in the images.

Figure 13 shows optical images for the T351 (a-b) and the T39 (c-d) for specimens peened with 1 and 6 GW/cm^2 after seven laser hits. At the lowest power density (1-18-7) the grains in the T351 appear more equiaxed after seven shocks than was observed after one shock (Figure 12a).

Similar to the case for a single shock, clear evidence of grain refinement was not found for the T39 material (Figure 13d) subjected to seven shocks. At the highest power density with the maximum number of hits a recast layer with a thickness of about 100 microns is found (Figure 13d).

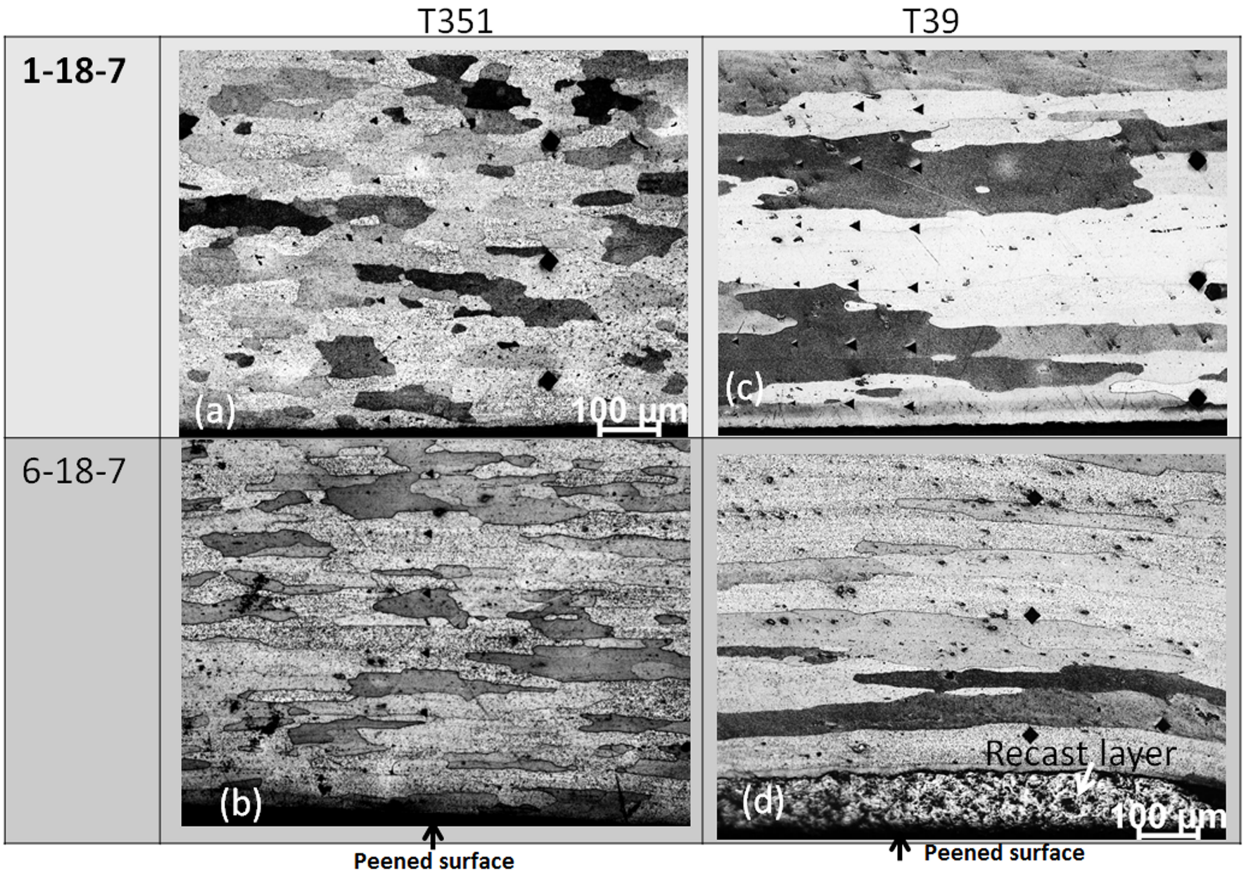

Figure 13: Microstructural images for the T351 (a-c); and the T39 (b-d) showing the effect of power density after seven impacts.

3.4 Results from instrumented indentation

3.4.1 Effect of Power Density on the Elastic Recovery

The elastic recovery h_e and the ratio h_e/h_{max} are useful experimental parameters to assess the material behaviour in response to peening, because these parameters can be directly obtained from the load-displacement curve and thus are not affected by measurement inaccuracy in the indentation area. Small errors generally occur while defining the area function for hardness calculation owing to the piling-up or sinking-in behaviour, particularly when residual stresses are present. Therefore, h_e and h_e/h_{max} parameters are presented in Figures 14a-d to show the effect of laser intensity. The unpeened h_e values are 325 and 340 nm for T351 and T39, respectively. The standard deviations for the T351 and T39 (at 6-18-1) are 3 nm and 6 nm, respectively. Higher values of elastic recoveries are found for the T39 because of its higher yield strength compared to the T351 (see Figure 3). The near-surface h_e values are about 355 nm for the T351 and 360-380 nm for the T39, levelling out at about 4 mm below the peened surface. Increased values of the elastic recoveries near the surface resulted from peening-induced plastic deformation. When the power density was doubled from 3 to 6 GW/cm^2, the T39 showed lower values of elastic recovery at the surface (Figure 15b). This difference (360 nm versus 380 nm) may be partly attributed to the combined thermal and mechanical effect. The formation of the recast layer shown in Figure 13d confirmed that the near-surface material was subjected to temperatures as high as the melting point of the alloy.

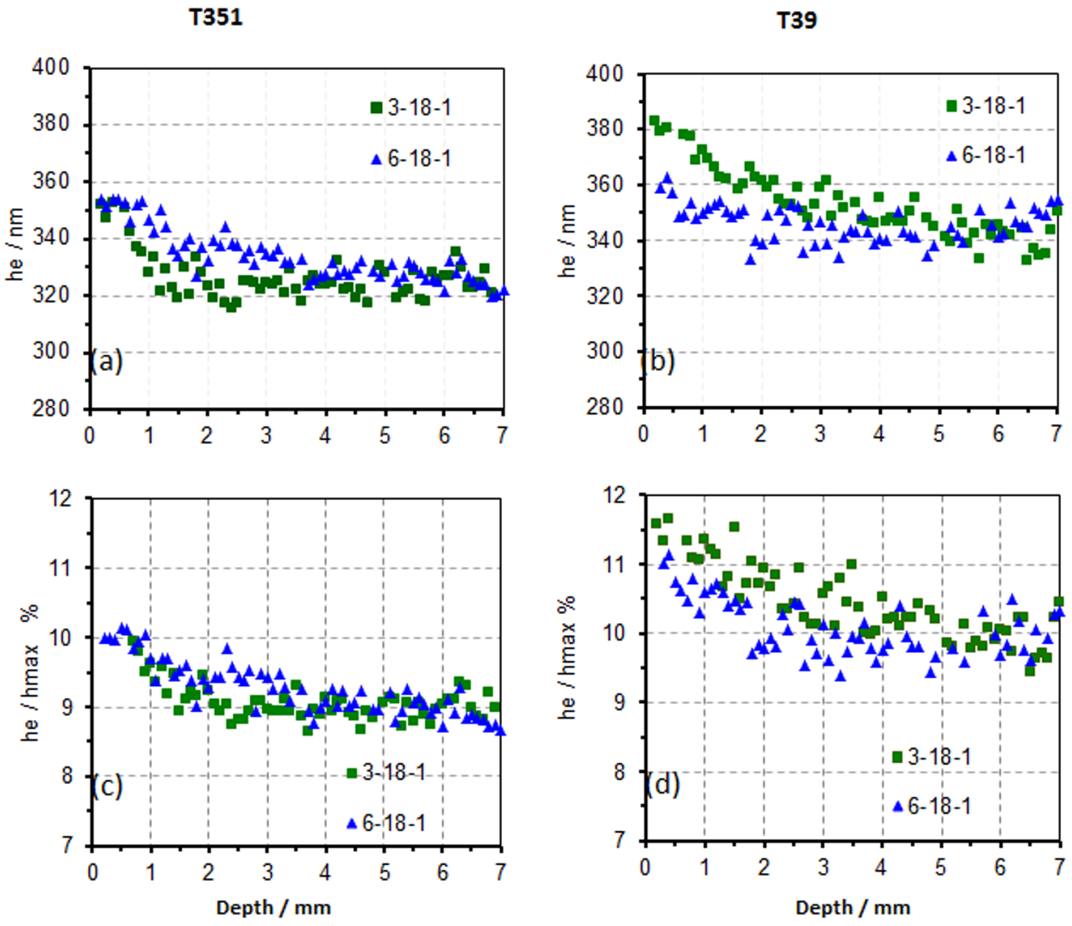

Figure 14: Effect of laser power density on the elastic recovery, and the ratio of elastic recovery to the displacement at maximum load for the T351 (a, c); and for the T39 (b, d).

Figures 14c and d show the ratio h_e/h_{max} as a function of depth for the two heat treatments. The slightly higher h_e/h_{max} observed for the T39 resulted from the 20% lower E/σ_y ratio (155 for the T39 and 194 for the T351, as shown in Table 1). From these plots we can infer:

1) The effects of peening diminish at about 4 mm below the peened surface.

2) The maximum increases in the near-surface values of h_e/h_{max} are 10% and 11.5% for the T351 and T39, respectively. The T351 showed no difference in h_e/h_{max} between 3 and 6 GW/cm^2, whilst the T39 actually showed slightly lower h_e/h_{max} values at 6 GW/cm^2.

Figure 15 presents the hardness results, normalized by the averaged far-field hardness, plotted as a function of depth. The averaged far-field hardness was calculated by averaging the hardness values of the last 10 indents created between 6 and 7 mm from

the surface. Figures 15a and b show a comparison of the effect of power densities of 1, 3, and 6 GW/cm^2 after a single laser impact for the T351 and T39 conditions. At 1-18-1, 5% hardness increase is found for the T351 which is further increased to 10% at 6-18-1; for the T39, the hardness was increased by 12% at 1-18-1 which was further increased to 18% at 6-18-1. The relative standard deviation for the T351 and the T39 were 2 and 3% respectively (calculated from the 1-18-1 hardness data points between 6 to 7 mm).

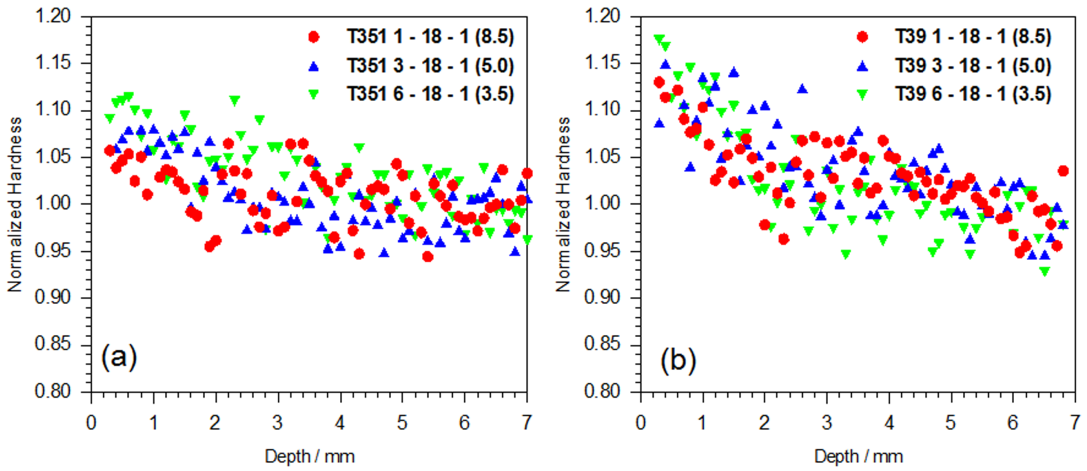

Figure 15: Effect of power density on the hardness of (a) T351 alloy and (b) T39 alloy

3.4.2 Effect of number of laser impacts

The elastic recovery plots presented in Figures 16a and b show the effect of number of laser impacts for the T351 and the T39 at 3 GW/cm^2 for one, four, and seven impacts. It is evident that the elastic recovery decreases with increasing number of impacts as there is less additional hardening following the effect of the first shock. This can be correlated with the increase of residual stresses seen (Figure 10c) with increasing laser impacts.

Our results were confirmed with similar measurements for the 6 GW/cm^2 peening (6-18-1, 6-18-4, and 6-18-7), as shown in the supplementary material, and additional Vickers hardness measurements.

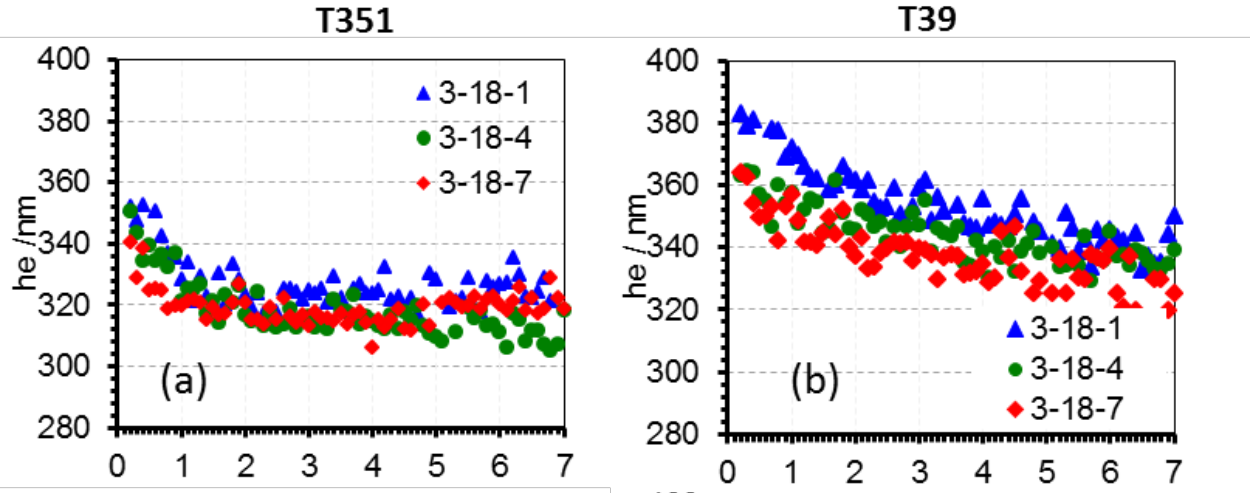

Figure 16: Variation of elastic recovery, h_e as a function of distance from the peened surface for (a) T351, and (b) T39 peened at 3 GW/cm^2

The normalized hardness profiles as a function of depth at 3 GW/cm^2 for one, four and seven layers are presented in Figures 17a and c for the T351 and the T39, respectively. For the T351, the hardness increased by 8% as compared with the unpeened material after one shot, and increased to 18% after four shots. No further hardness increase was obtained for seven shots. In contrast, the T39 showed a 14% hardness increase after the first shot, with no further increases evident after additional shots. Comparison between the two heat treatments shows that at 3-18-4 and 3-18-7 the T351 hardened slightly (~4%) more than the T39.

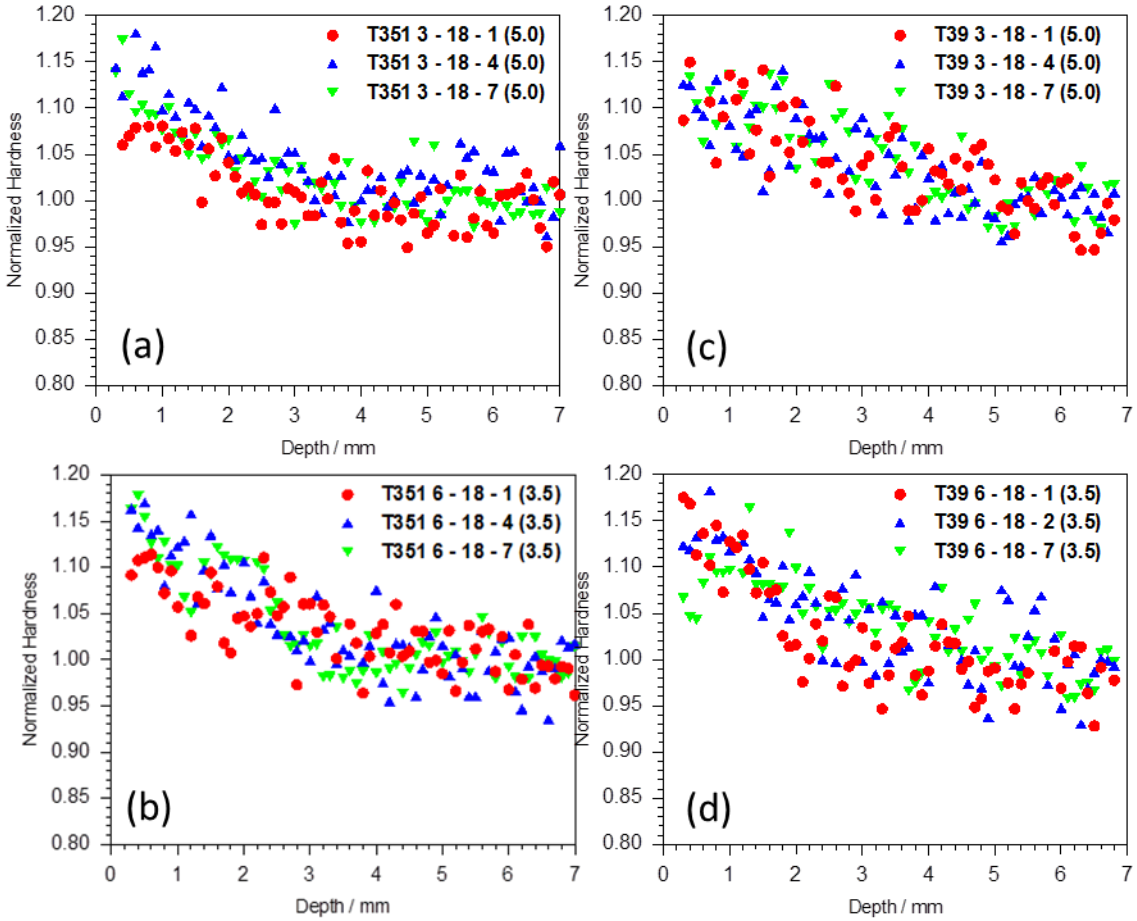

Figure 17: Effect of number of peening impacts on the hardness of (a) T351 alloy and (b) T39 alloy at 3 GW/cm^2; and (c) T351 alloy and (d) T39 alloy peened with a power density of 6 GW/cm^2.

When the power density was doubled to 6 GW/cm^2 (Figures 15c and d), the first shot resulted in a 10% hardening for the T351. An 18% hardness increase was observed after the fourth shot, but additional shots resulted in no additional hardening, similar to what was observed at 3 GW/cm^2. In contrast, while an 18% hardness was achieved for the T39 alloy (Figure 18d) after the first shot, additional hits resulted in a reduction of hardness near the surface.

4. Discussion

The correlation between residual stress generation and hardening for both heat treatment conditions is shown in Figure 18. From these plots, the following observations can be made:

1. From Figure 18, there seems to be an optimum peening condition that yields the best combination of compressive residual stress with strength, with 'underpeening or 'overpeening' giving poorer outcomes. For example, peening

with 6 GW/cm^2 results in almost 50% reduction in the surface compressive residual stresses as compared to peening at the lower intensities (Figure 18e). Corresponding hardness values are also reduced (Figure 18f). The extent of the surface effects is around 250 μm. The maximum hardening/residual stress invariably occurs beyond this depth.

2. For both tempers, the variation in subsurface peak hardness observed between 1, 3 and 6 GW/cm^2 after a single impact is small; the only noticeable difference is ~10% greater hardening in the T39, which can be attributed to the initial unpeened hardness state. In comparison to the unpeened condition, the T351 showed 8% hardening (see Figure 18a) which did not change even for a six-fold increase in laser power density. On the other hand, the T39 hardened by around 15%. The difference in hardening between the T39 and T351 is also relatively small considering the 20% difference in the unpeened yield strength between them. The hardening observed here is a result of plastic deformation, that decreases with increasing depth into the material.

   The residual stress results correlate with the hardness and microstructural changes caused by peening. In the T351, subsurface residual stresses are increased by 30% when the power density increases from 1 to 6 GW/cm^2 (Figure 18a). In contrast, for the T39, after the first impact at 6 GW/cm^2, higher subsurface residual stresses are generated (Figure 18a) owing to the higher yield strength and ultimate tensile strength. Thus the T39 can sustain higher levels of residual stresses. Seemingly, the yield strength difference between the tempers plays a significant role only at higher energies.

3. The number of laser impacts has a significant effect on the depth and the magnitude of the residual stress field and hardness. Both the values of maximum compression and the hardness gradually increase with increasing number of impacts in the T351 at all power densities. This is consistent with previous results: for example, Zhang *et al*. showed similar results in LSP of a magnesium alloy [13]. Maximum compressive residual stresses were found to be –350 MPa at 3-18-4 for the T351 and at 3-18-7 for the T39 (Figure 19b & e) with a small drop in compression near-surface. Therefore, these peening parameters are deemed to be the optimum for this material: the initial yield strength difference

between the tempers does not noticeably affect the residual stress or hardness response. Although, it was explained previously that the baseline yield strength before peening is a predominant factor in the residual stress/hardness after one laser impact, when a material is successively plastically deformed by laser-induced shock wave, it will harden until it reaches a saturation point. The T351 and T39 can have similar hardness/residual stress but significantly different microstructures (seen in Figure 14). The precipitation dynamics are likely to be different in the T39 compared to the T351 because of the cold working prior to ageing. This may be the reason why grain refinement was observed in the T351, and not the T39. Further work is required to understand this mechanism. Increasing the power density to 6 GW/cm^2 reduced the near-surface (up to 100 microns) residual stresses greatly and subsurface residual stresses slightly. Although no hardness data was available in this region, slightly lower hardness values were found for the T39 up to a depth of 300 microns.

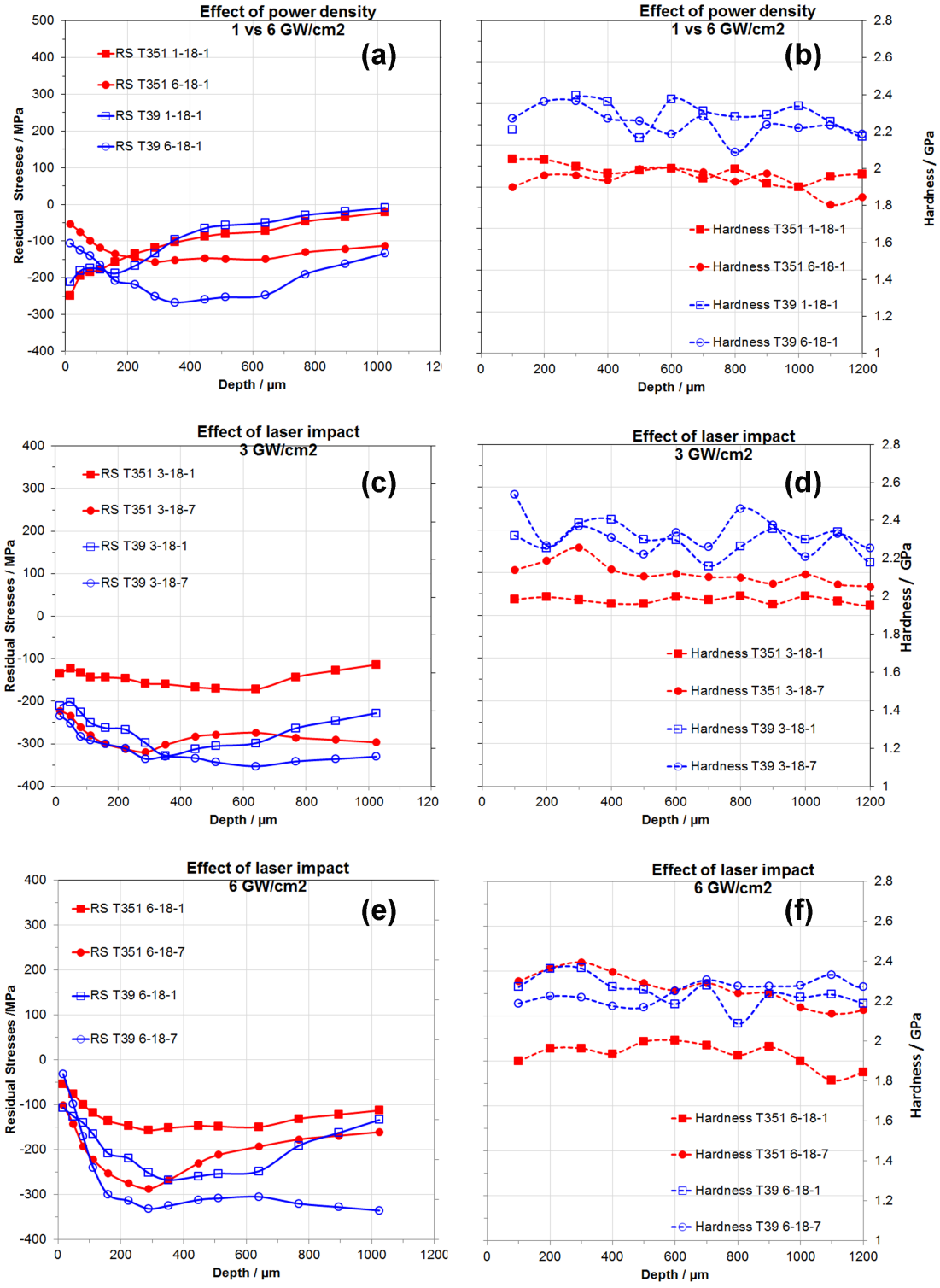

Figure 18: Correlation of hardness and residual stresses between the T351 and the T39: (a) comparison of the effect of power density after the first impact between 1 and 6 GW/cm²; (b) comparison of the effect of laser impact between 1 and 7, at 1 GW/cm²; (c) 3 GW/cm²; and (d) and 6 GW/cm². Solid lines plotted on the primary axis show the residual stress and dotted lines plotted on the secondary axis show the hardness variation through the depth up to 1000 µm. 'Red' closed markers are used to represent the T351 and 'Blue' open markers are used for the T39.

4. Although at the lowest laser intensity (1-18-1) the T39 hardens more compared to the T351, with increasing power density as well as the number of impacts the T351 continues to harden, surpassing the unpeened hardness of the T39, and ultimately reaching the peened hardening state of the T39 near the surface. The T39 would be expected to show lower hardening compared to the T351 owing to its lower hardening capacity (see Figure 3). The T39 did not show any significant variation in residual stresses near the surface up to 500 μm (Figure 19 c–d); however the peak compressive stress location was pushed to the subsurface with increasing number of impacts.

Conclusions

We have undertaken a comprehensive study of the effect of laser shock peening on two different tempers of aluminium alloy 2624. The two tempers, T351 and T39, have different yield and ultimate tensile strengths, and different hardening characteristics post-yield.

1. Laser shock peening induces compressive residual stresses at the surface for both tempers, with the magnitude of stress increasing with power density and number of shocks up to a saturation point which is approximately 3 GW/cm^2 for four to seven shocks. The magnitude of maximum compressive residual stresses are –350 MPa for both alloy tempers. The at-surface residual stress falls for the highest power density studied, 6 GW/cm^2, because of reverse yielding near-surface.
2. In general, the hardness is increased as a result of peening. The exception is that for high power densities, and particularly after multiple shocks, the T39 condition showed a drop in hardness near-surface. After a single laser shock, a 5% hardness increase was observed for the T351, increasing to 10% at 6 GW/cm^2. The T39 showed a maximum hardness increase of 18% at 6 GW/cm^2. Additional shocks increased the hardness further. For seven shocks, ~8% hardness increase was observed for the T351 at 1 GW/cm^2, which increased to 18% when the power density was doubled. Whilst cyclic softening could be a contributing factor, it appeared that there had been thermal damage to the surface, resulting in the formation of a recast layer.

3. Evidence of grain refinement was found for the T351 following peening, but no evidence of grain refinement was found for the T39.
4. The depth of the LSP-affected region increases with increasing power density, to a maximum of 4 mm depth.

Acknowledgements

This research study was sponsored by the Air Force Office of Scientific Research, Air Force Material Command, USAF, under grant number FA8655-12-1-2084, and the Air Force Research Laboratory's Aerospace Vehicles Directorate. The U.S. Government is authorized to reproduce and distribute reprints for Government purpose notwithstanding any copyright notation thereon. The views and conclusions contained herein are those of the authors and should not be interpreted as necessarily representing the official policies or endorsements, either expressed or implied, of the Air Force Office of Scientific Research or the U.S. Government. The authors would like to thank Dr Markus Heinimann at Alcoa Inc. (now Arconic) for the provision of the material studied in the project. Thanks are also due to Mr Pete Ledgard and Mr Stan Hiller at The Open University, Dr Philip Whitehead at Stresscraft, UK, and Mr Steve Allitt at Coventry University, for technical support. Special thanks are due to Dr Pratik Shukla for helpful discussion. MEF is grateful for funding from the Lloyd's Register Foundation, a charitable foundation helping to protect life and property by supporting engineering-related education, public engagement and the application of research.

References

[1] P. Peyre, R. Fabbro, Laser shock processing: a review of the physics and applications, Optical and Quantum Electronics, 27 (1995) 1213-1229.
[2] C.S. Montross, T. Wei, L. Ye, G. Clark, Y.-W. Mai, Laser shock processing and its effects on microstructure and properties of metal alloys: a review, International Journal of Fatigue, 24 (2002) 1021-1036.
[3] M. Dorman, M.B. Toparli, N. Smyth, A. Cini, M.E. Fitzpatrick, P.E. Irving, Effect of laser shock peening on residual stress and fatigue life of clad 2024 aluminium sheet containing scribe defects, Materials Science and Engineering: A, 548 (2012) 142-151.
[4] R.A. Brockman, W.R. Braisted, S.E. Olson, R.D. Tenaglia, A.H. Clauer, K. Langer, M.J. Shepard, Prediction and characterization of residual stresses from laser shock peening, International Journal of Fatigue, 36 (2012) 96-108.
[5] T. Sano, T. Eimura, R. Kashiwabara, T. Matsuda, Y. Isshiki, A. Hirose, S. Tsutsumi, K. Arakawa, T. Hashimoto, K. Masaki, Y. Sano, Femtosecond laser peening of 2024 aluminum alloy without a sacrificial overlay under atmospheric conditions, Journal of Laser Applications, 29 (2017) 012005.
[6] M.B. Toparli, N. Smyth, M.E. Fitzpatrick, Effect of Treatment Area on Residual Stress and Fatigue in Laser Peened Aluminum Sheets, Metallurgical and Materials Transactions A, 48 (2017) 1519-1523.
[7] ASTM E837-13a, Standard Test Method for Determining Residual Stresses by the Hole-Drilling Strain Gage Method, ASTM International, West Conshohocken, PA, 2013.

[8] P.V. Grant, J.D. Lord, P.S. Whitehead, Measurement Good Practice Guide No. 53: The Measurement of Residual Stresses by the Incremental Hole Drilling Technique, National Physical Laboratory, Teddington, UK, 2002.
[9] S. Suresh, A.E. Giannakopoulos, A new method for estimating residual stresses by instrumented sharp indentation, Acta Materialia, 46 (1998) 5755-5767.
[10] M.K. Khan, M.E. Fitzpatrick, S.V. Hainsworth, L. Edwards, Effect of Residual Stress on the Nanoindentation Response of Aerospace Aluminium Alloys, Computational Materials Science, 50 (2011) 2967-2976.
[11] M.K. Khan, M.E. Fitzpatrick, S.V. Hainsworth, A. Evans, L. Edwards, Application of synchrotron X-ray diffraction and nanoindentation for the determination of residual stress fields around scratches, Acta Mater., 59 (2011) 7508-7520.
[12] W.C. Oliver, G.M. Pharr, An improved technique for determining hardness and elastic modulus using load and displacement sensing indentation experiments, J. Mater. Res., 7 (1992) 1564-1583.
[13] Y. Zhang, J. You, J. Lu, C. Cui, Y. Jiang, X. Ren, Effects of laser shock processing on stress corrosion cracking susceptibility of AZ31B magnesium alloy, Surface and Coatings Technology, 204 (2010) 3947-3953.